

Article

# Wind Micro-Turbine Networks for Urban Areas: Optimal Design and Power Scalability of Permanent Magnet Generators

Marco Palmieri <sup>1,\*</sup>, Salvatore Bozzella <sup>1</sup>, Giuseppe Leonardo Cascella <sup>1</sup>, Marco Bronzini <sup>1</sup>, Marco Torresi <sup>2</sup> and Francesco Cupertino <sup>1</sup>

<sup>1</sup> Department of Electrical Engineering and Information Technology, Politecnico di Bari, 70126 Bari, Italy; salvatore.bozzella@poliba.it (S.B.); giuseppeleonardo.cascella@poliba.it (G.L.C.); marco.bronzini@poliba.it (M.B.); francesco.cupertino@poliba.it (F.C.)

<sup>2</sup> Department of Mechanics, Mathematics and Management, Politecnico di Bari, 70126 Bari, Italy; marco.torresi@poliba.it

\* Correspondence: marco.palmieri@poliba.it; Tel.: +39-080-569-3769

Received: 22 September 2018; Accepted: 13 October 2018; Published: 15 October 2018



**Abstract:** This work is focused on the design optimization of electrical machines that are used in small-scale direct-drive aerogenerators. A ducted wind turbine, equipped with a diffuser, is considered due to its enhanced power capability with respect to bare turbines. An annular type Permanent Magnet brushless generator is integrated in the turbine structure: the stator coils are placed in the internal part of the diffuser, whereas the permanent magnets are on an external ring connected to the turbine blade tips. Moreover, as regards the stator windings, the Printed Circuit Board (PCB) technology is investigated in order to exploit its advantages with respect to conventional wire coils, such as the increased current density capacity, the reduction of costs, and the enhanced precision and repeatability of the PCBs. An original design procedure is presented together with some scalability rules. An automated tool has been developed in order to aid the electrical machine designer in the first design stages: the tool performs multi-objective optimizations (using the Matlab Genetic Algorithm Toolbox), coupled to fast Finite Element analysis (through the open-source software FEMM) for the evaluation of the electromagnetic torque and field distribution. The proposed procedure is applied to the design of an annular PM generator directly coupled to a small-scale turbine for an urban application.

**Keywords:** electrical machines; renewable energy; ducted wind turbines; PCB winding; scalability; design automation; multi-objective optimization; FEA

## 1. Introduction

The development of renewable power generation systems is getting even more important in the last decades due to the increasing demand of electrical power and the increased attention towards the reduction of CO emissions [1]. In this framework, wind turbine systems can be considered to be one of the most promising technologies, as demonstrated by the huge penetration of such devices in the distribution and transmission networks in the north of Europe, United States (US), and China [2–4]. Installed wind power is currently larger than 540 GW and it is expected to exceed 700 GW by 2020 [5].

According to the power range, wind turbines can be classified as utility-scale systems (for power values above 1 MW), medium-scale systems (for power values usually between 100 kW and 500 kW and up to 1 MW), and small-scale systems (below 100 kW); aerogenerators below 1 kW, are sometimes defined as micro-scale or even pico-scale turbines [6].

Small wind turbines represent a viable solution to face the energy demand of urban or rural areas [7], because they can be installed with a limited environmental impact. Moreover, with respect to photovoltaic systems, they require a reduced surface for the same produced power and ensure higher efficiency.

The electro-mechanical conversion system of a conventional wind generator usually consists of three main parts: the turbine, the electrical machine operated as generator, and a mechanical gearbox in between. The mechanical gearbox is mainly used to increase the rotational speed of the electrical machine; for a given power to be processed, this allows for using a smaller generator with reduced volume and cost of this component. However, the adoption of a gearbox for adapting the mechanical speed presents several drawbacks: firstly, size and weight of the overall conversion system are increased because the wind turbine nacelle has to accommodate a further device, while the reliability and the dynamic behavior are worsened. Secondly, the gearbox generates noise and increases the conversion losses, thus reducing the global efficiency; moreover, it requires a regular maintenance and lubrication, which means further costs and can constitute a significant disincentive especially for off-shore installations [8].

A possible way to overcome the aforementioned issues is the adoption of direct-drive solutions, with the electrical machine coupled to the turbine directly. The main advantages of this architecture are higher efficiency, energy yield, and reliability, as well as reduced noise and maintenance costs [8]. However, this kind of solutions requires a generator with large diameter and airgap plus a power electronics converter designed for the full rated power; both of these features are rather expensive [9,10].

In the literature different topologies of electrical generators have been studied, highlighting advantages and limitations of each solution [2,10,11]. The doubly fed induction machine is a widely adopted topology for geared wind generators with a multi-stage gearbox: the stator can be connected to the grid through a power transformer, without interposing switching devices; the rotor is equipped with a power electronics converter that controls the rotor frequency [10]. The power converter is usually designed for about one-third of the generator power capacity, thus reducing losses and costs that are associated to this component; moreover, the converter allows the reactive power compensation as well as a smooth grid connection. The main drawbacks of this architecture are the presence of the gearbox, the power losses, and the maintenance costs that are associated to the slip rings on the rotor and the necessity of dedicated protection strategies able to prevent the converter destruction, under grid faults, due to the large amount of rotor currents [10].

As regards direct-drive aerogenerators, the preferred electrical machines topologies are the wound rotor synchronous machines and the Permanent Magnet (PM) brushless machines [6,10]. The former solution presents a DC winding on the rotor carrying the excitation current; whereas, in the latter, the excitation field is provided by permanent magnets. PM machines are very attractive because, with respect to wound rotor ones, they guarantee high efficiency and torque density, no excitation losses, and enhanced reliability due to the absence of slip rings; moreover, they do not require a power conversion device connected to the field winding. The main drawbacks are the cost of the PM, which is high and volatile, and the demagnetization issues at high temperatures [9,10].

A recent example of wound rotor synchronous machines for wind power generators is reported in [12], where a new geometry aimed at simplifying the insertion\removal of rotor windings was presented. The rotor shape was obtained through optimizations based on the surrogate method and the simulation results were experimentally validated. With respect to traditional rotors, the asymmetrical one that was proposed in [12] shows similar performance but guarantees, at the same time, reduced maintenance and repair costs. A further original wound field synchronous machine for wind applications is proposed in [13], where the authors presented a half-wave rectified brushless excitation system: in [13] the machine structure recalls that of a conventional salient pole synchronous generator, but the stator slots accommodate both the armature and the excitation windings; moreover, the rotor

field winding is short-circuited by a diode, thus the field flux is produced by rectifying the induced voltage through the diode without adopting slip rings.

Plenty of PM synchronous generators, whether axial flux or radial flux machines, have been presented in the literature in the last decades [14–17]. Moreover, the research is focused on non-conventional configurations that were aimed at improving the overall performance or reducing the manufacturing issues. The work reported in [16] presents a transverse flux PM disk generator, whose main feature is the adoption of modular H-shaped stator cores made by two T-shaped cores plus a permanent magnet in order to simplify the assembling process. In [17], the design of an axial-flux PM generator with a double rotor and one yokeless segmented stator is performed by means of a multi-objective optimization aimed at maximizing the efficiency and reducing the cost of active materials. A comprehensive methodology for the design of a radial flux iron-less PM machines is presented in [14]: three-dimensional FEA is used and the simulations are validated after experimental tests; the adopted topology has solenoid-shaped coils and a simple mechanical design so to guarantee ease of maintenance. A different approach is adopted in [15], where the authors investigate the electromagnetic and mechanical aspects of radial flux double rotor PM air-cored generators through an optimization algorithm coupled to analytical models in order to reduce the computational burden.

As regards the stator coils, the adoption of planar windings realized using Printed Circuit Board (PCB) coils can be a viable alternative to conventional concentrated windings made by wires. One of the main advantages of these windings is their enhanced current carrying capacity, about ten times greater with respect to traditional wire-wound coils [18,19]; this leads to more compact and lighter solutions. Secondly, the manufacturing process of these coils is widely consolidated and guarantees high accuracy and reliability with reduced costs, especially for large scale production [19]. Moreover, PCBs allow for optimizing the geometry and the shape of the windings and guarantee, at the same time, very high precision and full repeatability in the traces' arrangement. Finally, due to the possibility of reducing the thickness of the PCB traces, the frequency dependent phenomena, like the proximity effect, become negligible, with a strong impact on the overall efficiency at higher electrical frequencies. All of the aforementioned advantages have increased the interest of both industry and academia towards the adoption of printed circuit boards for the design of non-conventional electrical machines. In [20], a prototype of an integrated motor-pump structure made of an axial flux PM machine with PCB windings is built and tested; in that arrangement and with a very limited volume, a vortex type impeller is located on the magnet periphery and the fluid flow is controlled by adjusting the motor speed. An axial flux single phase iron-less PM generator with PCB stator is proposed in [21], with the aim of developing a zero cogging torque solution for small marine energy conversion systems. In [22] a novel flexible PCB winding for a slot-less linear PM motor is investigated and an original configuration made of rhomboidal and triangular coils is proposed in order to reduce the end-windings. A further example is proposed in [23], where the armature of a double-sided linear brushless DC motor is constituted by PCB coils in order to reduce the mechanical time constant and to improve the dynamic performance of the machine. Due to the enhanced heat distribution, a current density up to 100 A/mm<sup>2</sup> was reached in [23].

The choice of the proper machine topology is not univocal and is mainly related to the specific application and power rating. In this work, the attention is focused on small-scale aerogenerators without gearboxes: a ducted wind turbine is considered as prime mover, since it guarantees to better exploit the kinetic energy of the wind for a given turbine volume, as reported in the following sections. The electrical generator is an annular PM brushless machine designed so to be integrated within the turbine envelope; in particular, the adoption of PCB windings that are located in the inner part of the diffuser structure is investigated. Since one of the main issues of the PM generators is the cost of the active parts, an original design procedure that was aimed at minimizing the volume of the permanent magnets and copper has been developed: the proposed procedure, embedded in a Matlab script, is based on a multi-objective optimization performed through genetic algorithms coupled to finite element analysis (FEA).

The work is organized as follows: an overview of the considered direct drive small-scale wind generator is presented in Section 2. In Section 3, some useful analytical rules for the power scalability of the electrical machine are provided, while the proposed automated design tool is presented in Section 4. Finally, Section 5 reports the simulation results of the considered case of study, concerning a kW range Permanent Magnet generator for urban applications.

## 2. Main Components of the Proposed Electromechanical Energy Conversion System

The architecture of the direct-drive wind generation system under investigation is composed by two key parts: the horizontal axis ducted turbine and the PM brushless generator.

### 2.1. Ducted Wind Turbine

Different one-dimensional (1D) theoretical models have been proposed in the literature in order to predict the power production of wind turbines, with particular reference to shrouded or diffuser-augmented ones [4,24–27]. The turbine is seen as an actuator disc and the flow over the disk is supposed to be ideal (i.e., without a rotational velocity component and frictionless). As shown in Figure 1, the disc reduces the wind speed from  $v_a$  upstream to  $v_p$  at the rotor and then to  $v_o$  downstream; consequently, the pressure rises at the upstream section of the rotor, then it has a drop across the disc and finally increases again downstream [27]. These changes in pressure and speed inside the streamtubes both upstream and downstream the rotor can be described by the Bernoulli's equation.

In order to consider ducted wind turbines, a reformulation of the conventional blade element momentum theory was proposed in [28]. In this case, CFD simulations have been carried out based on the solution of the steady two-dimensional Reynolds-averaged Navier–Stokes equations for axisymmetric swirling flows. Moreover, the turbine effect on the flow field has been accounted for by means of source terms for the momentum equations solved inside the domain swept by the rotor; this allows for avoiding expensive mesh refinement near the actual rotor blades, thus reducing the computational burden.

For horizontal axis bare turbines, the theory that was proposed by Lanchester, Betz, and Joukowski established the maximum energy extractable by a turbine in an open flow [27]: this value, known as the Betz limit, is equal to 0.59 times the kinetic energy of the wind.

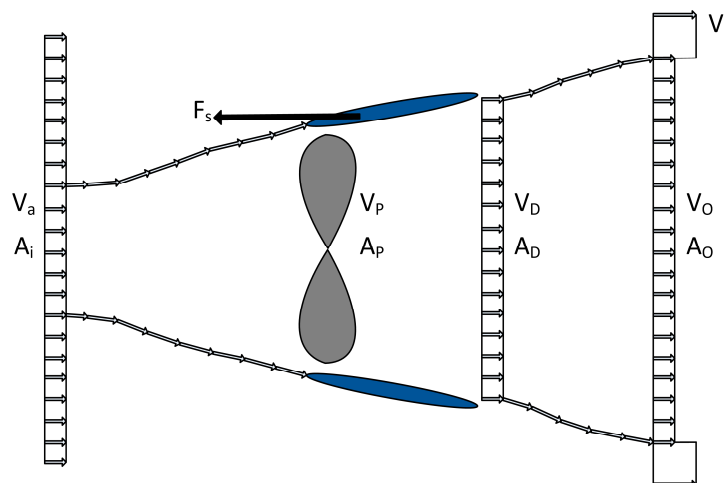


**Figure 1.** Model of a ducted turbine for the calculation of the extractable power from the wind.

Ducted/Shrouded Horizontal Axis Wind Turbines (S-HAWT) or Diffuser-Augmented Wind Turbines (DAWT) allow for enhancing the power output with respect to conventional or bare wind turbines, for a given rotor size [24–27]. In fact, the presence of the diffuser can provide an increase in the mass flow rate through the turbine blades, which produces a significant augmentation of the power

coefficient  $C_p$  referred to the rotor swept area [26]. The aforementioned power coefficient expresses the relation between the obtainable mechanical power and the power contained in the wind passing a reference area (conventionally the rotor swept area) with a given wind velocity [4].

In conclusion, the main advantages of DAWTs include the acceleration of the wind speed and the noise reduction with respect to the conventional bare turbines. The drawbacks are related to the extra weight and cost due to the presence of the diffuser; these structural and economic issues act as a restraint in the development of utility-scale wind turbines, whereas they constitute an affordable challenge for small- and micro-scale systems [24].

## 2.2. Permanent Magnet Generator

In this work, the adoption of a permanent magnet synchronous machine directly coupled to the turbine is proposed and investigated: this topology exhibits high torque density and power factor, thus allowing for a weight reduction of both the generator and the power converter with respect to other competitors for a given target power.

The selected generator is a three-phase surface mounted PM brushless machine, whose schematic representation, for the simple case of a two poles machine, is reported in Figure 2.

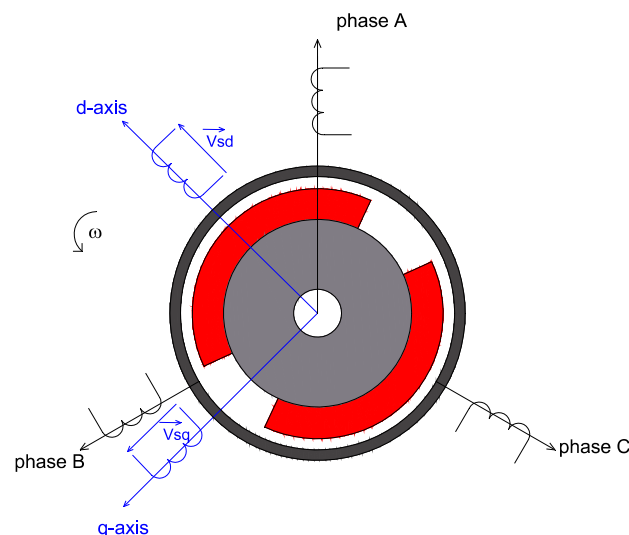


**Figure 2.** Schematic representation of a two poles three-phase brushless Permanent Magnet (PM) machine.

Considering the dq reference frame synchronous with the rotor, the machine model in vectorial notation can be expressed by the following Equation (1):

$$\vec{v}_{sdq} = R_S \cdot \vec{i}_{sdq} + \frac{\partial \lambda_{dq}}{\partial t} + j\omega \lambda_{dq} \quad (1)$$

where  $\vec{v}_{sdq}$ ,  $\vec{i}_{sdq}$ , and  $\lambda_{dq}$  are the voltage, current and flux linkage components, respectively,  $R_S$  is the phase resistance and  $\omega$  is the angular speed.

The machine considered here, is integrated within the ducted turbine structure: the presence of the diffuser is exploited to install the stator windings, while the rotor is made with a ring that is connected at the turbine blade tips, where the permanent magnets are allocated. The three-dimensional (3D) model of the proposed diffuser is shown in Figure 3, while the adopted architecture is reported in Figure 4.



Figure 3. Render of the diffuser.

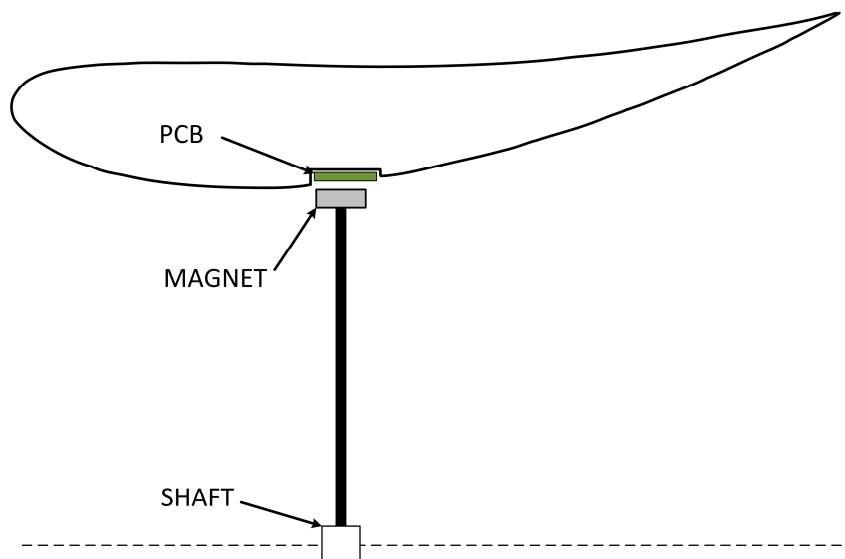
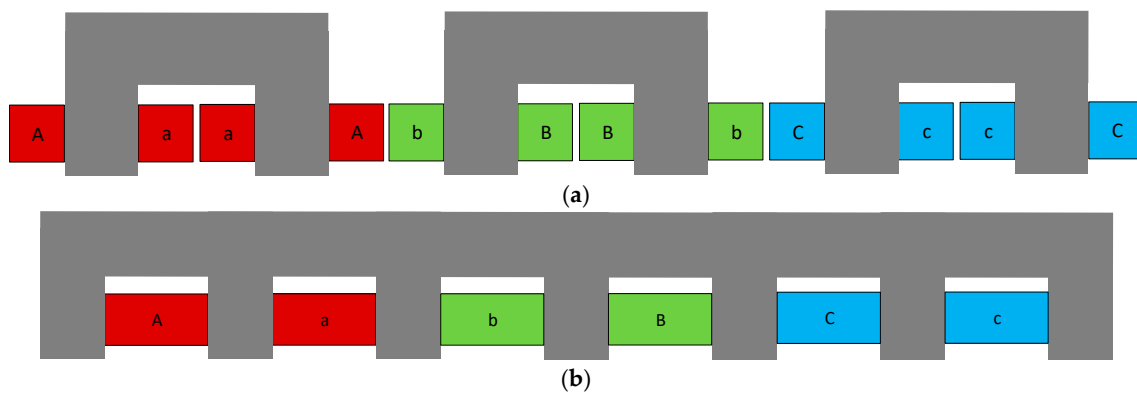


Figure 4. Concept of the annular PM machine with the Printed Circuit Boards (PCB) integrated in the diffuser of the ducted turbine.

As regards the stator coils, concentrated windings made by PCBs are investigated: for this type of machine, a Double Layer (DL) configuration is adopted while considering a 12/10 slot/pole combination.

The adoption of a DL winding for the selected slot/pole combination, even though slightly reduces the winding factor, guarantees the following advantages with respect to a Single Layer (SL) one:

- a segmented back iron, composed by one U-shaped core for each phase coil, can be used for the stator (as shown in Figure 5a); this solution allows to reduce the weight of the stator yoke and makes easier the manufacturing and assembly process, especially for machines with large diameters; and,
- for a given number of turns and thickness of the copper traces, the dimensions of the PCB in the axial direction can be shortened (as schematically shown in Figure 6); this is due to the reduction of the non-active parts of each phase coil.



**Figure 5.** Segmented stator yoke for double layer winding (a); and, continuous yoke for single layer winding (b).

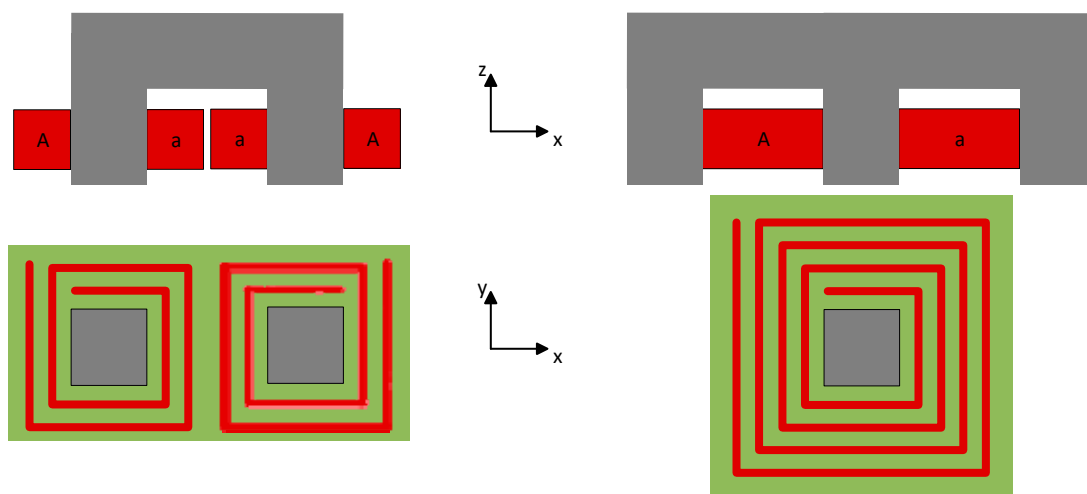


**Figure 6.** PCB arrangement and overall dimensions: double layer winding (left); single layer winding (right).

In small-scale wind turbines, the circumferential length at the tips of the rotor blade is relatively high and the axial length of the active part of the electrical machine (that is the axial length of the permanent magnets) will be limited to a few millimeters. Then, the total axial length of the PCB coils could be drastically reduced thanks a double layer arrangement of the stator windings. The Stator joke in Figures 5 and 6 includes back-iron and teeth by way of example only. In the following, in order to simplify the construction of the prototype, will be considered in both ironless stator structure and stator magnetic circuit limited to the back-iron (teeth-less stator).

### 3. Scalability Rules

A study on the power scalability of the aerogenerator is reported in the following in order to obtain a set of equations that relates the main geometrical dimension to the achievable output power. Starting from the aerodynamic relationships of the turbine and using the Betz theory, the extractable power from the wind is obtained by (2):

$$P = \frac{1}{2} C_P \rho A v_a^3 = \frac{1}{2} C_P \rho \frac{\pi}{4} D^2 v_a^3 \quad (2)$$

where  $A$  is the wind turbine rotor swept area and  $D$  its diameter,  $v_a$  is the wind speed upstream the streamtube,  $\rho$  is the air density, and  $C_P$  is the power coefficient.

For a target power  $P$  developed by the turbine, Equation (2) can be reversed so to calculate the diameter  $D$  of the electrical machine, as in (3):

$$D = \sqrt{\frac{P}{\frac{1}{2}C_P\rho\frac{\pi}{4}v_a^3}} \quad (3)$$

For the determination of the axial length  $L$ , it can be useful to consider the relation between the linear force density and the output torque  $T$ ; the former is defined as the ratio between the force at the airgap  $F$  and the rotor circumference  $C$  (with radius  $R$ ); its expression is reported in (4):

$$\frac{F}{C} = \frac{\frac{T}{R}}{2\pi R} = \frac{T}{2\pi R^2} \quad (4)$$

Considering the expression of the Tip Speed Ratio  $\lambda$ , defined as the ratio between the rotor tip speed and the wind speed upstream the streamtube, reported in (5), the torque produced by the electrical machine can be written, as in (6):

$$\lambda = \frac{\omega \cdot R}{v_a} \quad (5)$$

$$T = \frac{P}{\omega} = \frac{\frac{1}{2}C_P\rho\pi R^2 v_a^3}{\frac{\lambda v_a}{R}} = \frac{\frac{1}{2}C_P\rho\pi v_a^2}{\lambda} R^3 \quad (6)$$

By substituting (6) in (4) and considering (3), the ratio  $F/C$  as function of the output power is obtained (7):

$$\frac{F}{C} = \frac{T}{2\pi R^2} = \frac{\frac{1}{2}C_P\rho\pi v_a^2}{\lambda} R^3 \cdot \frac{1}{2\pi R^2} = \frac{C_P\rho v_a^2}{4\lambda} R = \frac{C_P\rho v_a^2}{4\lambda} \sqrt{\frac{P}{\frac{1}{2}C_P\rho\pi v_a^2}} = \sqrt{\frac{C_P\rho v_a^2}{8\pi\lambda^2}} \sqrt{P} = k\sqrt{P} \quad (7)$$

The electromagnetic torque produced by the generator is proportional to the  $D^2L$  product (being  $D$  the rotor diameter and  $L$  the axial length of the machine). Therefore, the ratio between the desired torque and the torque of a baseline machine can be written, as in (8):

$$\frac{T}{T_0} = \frac{D^2L}{D_0^2L_0} \quad (8)$$

where the subscript "0" indicates the baseline machine, taken as a reference. From the combination of Equations (7) and (8), the relationship between the linear force density and the output power of a machine with respect to the base one, can be expressed by (9):

$$\frac{\frac{T}{2\pi R^2}}{\frac{T_0}{2\pi R_0^2}} = \sqrt{\frac{P}{P_0}} \quad (9)$$

Finally, Equation (9) can be rearranged, considering (8), so to obtain (10) and (11), which relate the output power  $P$  to the axial length  $L$ :

$$\sqrt{\frac{P}{P_0}} = \frac{\frac{T}{2\pi R^2}}{\frac{T_0}{2\pi R_0^2}} = \frac{T}{T_0} \cdot \frac{R_0^2}{R^2} = \frac{D^2L}{D_0^2L_0} \cdot \frac{D_0^2}{D^2} = \frac{L}{L_0} \quad (10)$$

$$L = \frac{L_0}{\sqrt{P_0}} \sqrt{P} \quad (11)$$

Starting from a reference machine, on the basis of Equations (11) and (3), in a preliminary stage it is possible to scale the axial length of the machine so to obtain the desired power  $P$ . On the

contrary, the diameter determined by the Equation (3) should remain constant because it depends on fluid-dynamic considerations related to the turbine.

The proposed design procedure is based on the sizing of the baseline machine with the aid of optimization algorithms, so as to find the most convenient balance between copper and PM mass. Once the optimized baseline electrical machine is obtained, it could be modified using the scaling rules that are shown in this section so as to fit it with a wind turbine with a different power. One of the most interesting considerations that can be made on the basis of Equation (11) is that as the power increases, despite the increase in the circumference of the electrical machine, the axial length must increase with the square root of the power. This implies that the proposed constructive solution based on annular electrical machines, will be easily applied on micro wind turbines. For higher power ranges, the mass of permanent magnets could lead to structural problems difficult to be solved.

#### 4. Automated Design Tool

An automated tool for the optimal design of the electrical machine has been developed. The tool, implemented in the Matlab environment, allows for performing multi-objective optimizations using the Nondominated Sorting Genetic Algorithm NSGA II [29] embedded in the Matlab Optimization Toolbox. A finite element analysis is performed for the computation of the electromagnetic torque and the magnetic field distribution; at this purpose, the tool is interfaced with the free software FEMM [30]. The tool allows the design of annular type PM machines with inner rotor and concentrated windings on the stator core made by Printed Circuit Boards (PCB); the authors are currently working towards its extension to different machines topologies and PM arrangements.

##### 4.1. Multi-Objective Optimization

The adoption of multi-objective optimization aided by finite element analysis is a powerful tool for a large class of engineering problems; recent examples of similar procedures applied to the design of electrical machines are reported in [31–38]. One of the main drawbacks that is related to this approach is the required computational burden, which highly increases with the number of the cost functions and the dimension of the search space; moreover, the adoption of FEA furtherly lengthen the time required for evaluating each machine.

After the guidelines reported [31,33], in order to reduce the computational burden and the simulation time, the following approach is adopted here:

- two-dimensional (2D) magneto-static simulations are performed, considering few equally spaced rotor positions along one pole pitch;
- the electrical machine geometry is described by a limited number of parameters;
- a reduced portion of the entire geometry is analyzed, taking advantage of the machine symmetries; and,
- the computation is parallelized among all the cores of a workstation through the parallel toolbox provided by Matlab.

Due to the aforementioned features, the time required to analyze a single candidate machine is about 2 s on a quad-core workstation.

##### Meta-Heuristic Algorithm

The Nondominated Sorting Genetic Algorithm NSGA II [29] is a meta-heuristic population-based algorithm that iteratively modifies a set of candidate solutions according to probabilistic rules in order to find the global minimum of the chosen cost function [31,39]; the general scheme of a population-based algorithm is reported in Figure 7.

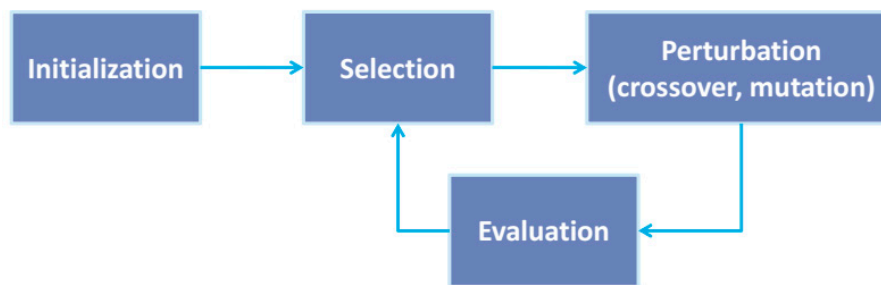


Figure 7. General scheme of a population-based algorithm [31].

Dealing with multi-objective problems, the concept of dominance is introduced in order to identify the “optimal” solutions: at each generation, a given solution is non-dominated if it is not possible to find other solutions with better values of all the cost functions; all of the solutions are ranked according to their non-domination level based on the selected cost functions [29]. The set of the non-dominated solutions constitutes the Pareto front and it is ranked 1; excluding the sub-set ranked 1, the remaining non-dominated solutions constitute the front ranked 2, and so on. Figure 8 illustrates this concept for a two-objective optimization.

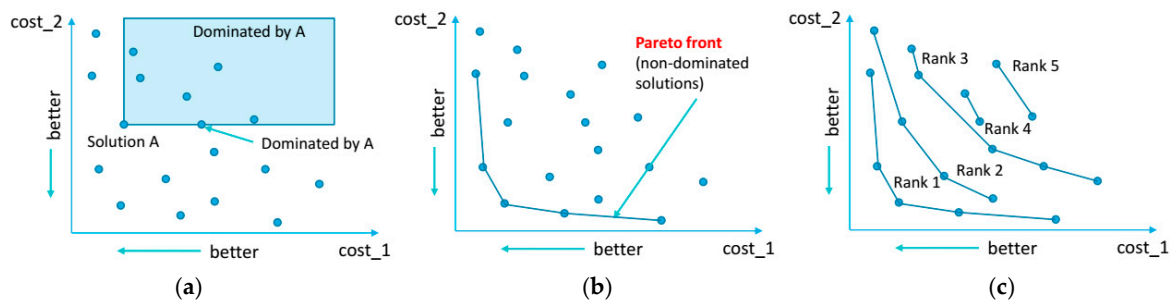


Figure 8. Multi-objective optimization: definitions of dominance criterion (a), Pareto front (b), and ranking of Pareto fronts (c) [31].

A single  $i$ -th iteration of the NSGA II algorithm is illustrated in Figure 9 and schematically exposed in the following; whereas, a complete description is reported in [29,31]:

1. a combined population  $CP(i)$  is formed considering a set  $P(i)$  of  $N_{pop}$  solutions originated from the  $(i - 1)$ -th iteration and a second set  $Q(i)$  of  $N_{pop}$  solutions obtained from  $P(i)$ , through crossover and mutation;
2. the population  $CP(i)$ , whose size is  $2N_{pop}$ , is sorted according to the non-domination criterion; therefore, a rank is assigned to each solution based on its non-domination level;
3.  $N_{pop}$  solutions are collected, starting from the 1st rank, in order to form the set  $P(i + 1)$ ; if the number of solutions belonging to the 1st rank is less than  $N_{pop}$ , the remaining candidates are collected from the subsequent non-dominated set (i.e., the 2nd rank) and so on until the size  $N_{pop}$  is reached; and,
4. the combined population  $CP(i + 1)$  for the  $(i + 1)$ -th iteration is finally obtained considering the combination between the population  $P(i + 1)$  and the population  $Q(i + 1)$  originated from  $P(i + 1)$  through crossover and mutation.

The optimization run stops when a preset termination criterion is reached (e.g., the maximum number of generations); at the end, the tool returns a graph with all the non-dominated solutions constituting the Pareto front in the selected objectives plane. The proposed tool acts as a decision support system, because, at the end of the optimization run, the choice of the final machine among the Pareto optimal solutions lies with the designer; since all the found solutions are equally good with

respect to the multi-objective problem, a human interaction is necessary in order to evaluate how much each objective function can be sacrificed for the particular application.

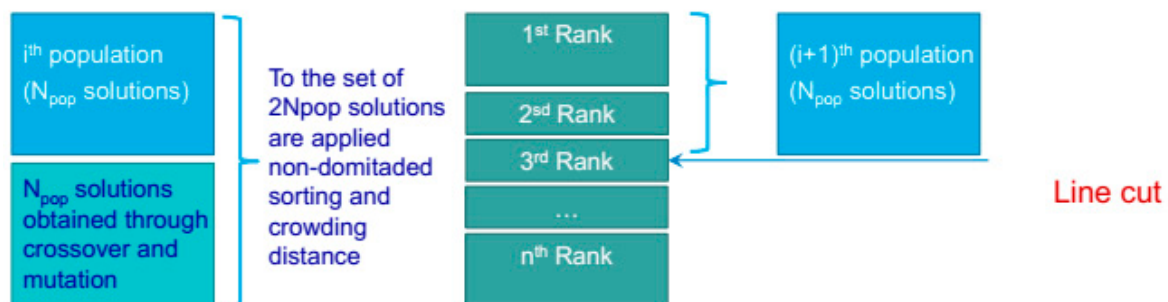
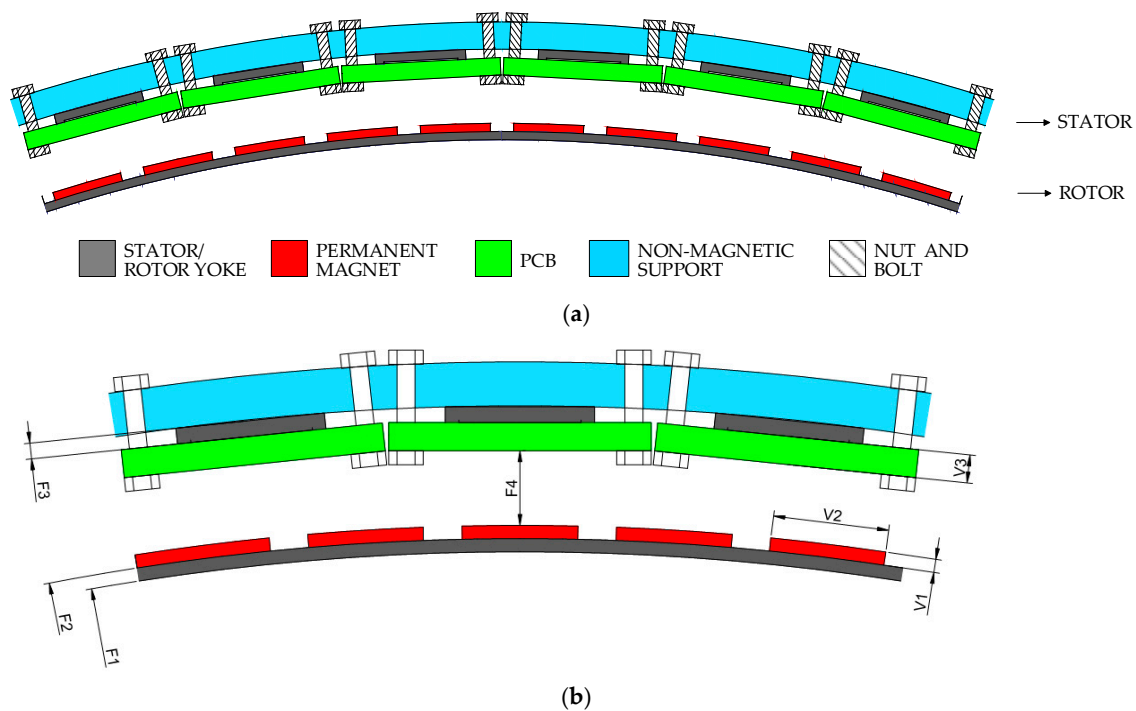


Figure 9. *i*-th iteration of the optimization algorithm [29,31].

#### 4.2. Machine Parameterization

The sketch of one module of the annular PM machine is reported in Figure 10a. The electrical machine is automatically drawn starting from a simple parameterization: in this study, the rotor radius (F1 in Figure 10b) and the airgap thickness (F4 in Figure 10b) are fixed according to mechanical constraints that are related to the ducted turbine; the optimization algorithm varies the magnets radial thickness (V1 in Figure 10b) and arc (V2 in Figure 10b), as well as the thickness of the PCB traces (V3 in Figure 10b) and computes the electromagnetic torque through finite element analysis in order to account for the system non-linearities. The current density has been taken equal to 10 A/mm<sup>2</sup> and the copper filling factor within the PCB cross section is considered as equal to 0.4. Such values are conservative estimates based on experience and validated by PCB manufacturers. Under these assumptions there is a linear relation between the PCB radial thickness and the machine current. The PCB coils are realized using copper layers with thickness usually below 140 μm isolated by 200 μm fiberglass layers. Once these manufacturing details are selected, it is possible to determine the number of layers and the number of turns for each layer. To limit the number of turns on each PCB layer, the modules belonging to the same stator phase are usually connected in series. A turn to turn isolation of 0.2 mm is needed among turns on the same layer, then a high number of turns would reduce the copper filling factor. The axial length *L* is adapted so to match the target torque  $T_{target}$ , selected on the basis of the wind turbine specifications. The thickness of the rotor and stator back-iron have been selected by some tentative FEA simulations before optimization. It was evidenced that the influence of back-iron thickness variations on average torque is evident only when the thickness is very limited, below manufacturing tolerances for the considered torque range. Each machine FEA analysis is then realized considering unity machine axial length ( $L_1 = 1$ ) to calculate the developed electromagnetic torque  $T_1$ . Then, the machine axial length is calculated as  $L = L_1 \frac{T_{target}}{T_1}$ . It is worth underlining that 2D FEA analysis are considered, then the machine end effects are neglected. Once the machine axial length is known, it is possible to calculate actual size and mass of the active parts (i.e., copper, iron, permanent magnets). The developed tool allows to define different materials for the stator and rotor cores, therefore both iron and ironless stator and rotor cores can be easily analyzed.



**Figure 10.** Sketch of one module of the annular PM machine (a) and detail of the main geometric parameters (b). The quantities  $F_i$  are fixed, the quantities  $V_i$  are varied during the optimization run.

#### 4.3. Cost Functions

The number of the objective functions has to be carefully chosen while considering the proper tradeoff between performance and computational burden: a high number of cost functions to be minimized/maximized simultaneously would be useful in order to account for different design issues at the same time; nevertheless, each additional objective function adds extra computational costs. Moreover, if the number of cost functions is greater than three, a very large population is required to correctly perform the optimization and the Pareto front is difficult to visualize [31,34,37].

Here, for sake of simplicity and readability of the results, a two-objective optimization is performed. Differently from the approach adopted in other works dealing with the design of electrical machines through multi-objective optimization [31,33–37], the cost functions that were selected for this particular application are the weight of the permanent magnets and the weight of the copper. As explained in the section dedicated to the machine parameterization, the axial length of the machines is adapted so to match the target torque  $T_{target}$ , and then all of the machines in the Pareto front will share the same torque and the same current density.

The adoption of the aforementioned cost functions for the optimal design of an electrical machine is one of the original contributions of this work; moreover, this choice is particularly smart because it provides a quick overview on different design issues at the same time:

1. the material cost, which is proportional to the weight for both the PMs and the copper, is indirectly considered; and,
2. the impact of the mechanical issues related to the rotor integrity, which are proportional to the rotor mass, can be estimated.

Therefore, the obtained graph can be a valid support during the design stage: according to the specific requirements, the designer will be able to select the proper machine deciding whether to favor efficiency (at the expense of the weight of the rotating parts) or to privilege the structural robustness (reducing the mechanical issues), or, finally, to choose the machine with the best compromise between performance and total costs. A flow chart of the proposed design methodology is reported in Figure 11.

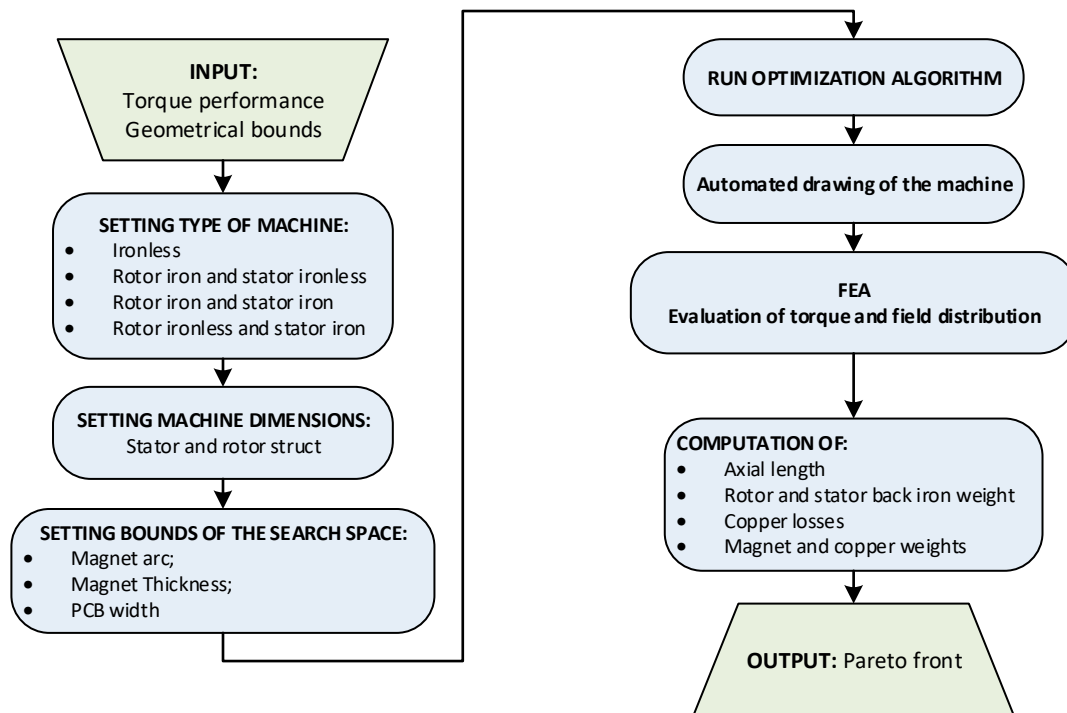


Figure 11. Flowchart of the proposed design procedure.

## 5. Case of Study

The procedure described in the previous section is applied to the design of an annular PM machine to be integrated in a micro-scale horizontal axis ducted wind turbine with rated power equal to 1 kW. The target values for the mechanical speed and the electromagnetic torque, chosen on the basis of the selected turbine, are equal to 662 rpm and 14.4 Nm, respectively. After some preliminary considerations, the airgap thickness is fixed to 10 mm, while the rotor diameter is set to 1440 mm according to Equation (3), where a wind speed equal to 10 m/s and a coefficient  $C_p$  equal to 1 are considered. The stator windings, placed on the inner surface of the diffuser, are realized using PCB concentrated coils in order to increase the current density and consequently reduce the copper weight with respect to standard wires; high strength permanent magnets (NdFeB 40 MGOe) are used so to enhance the power density. In order to improve the winding factor, the combination 10 poles/12 slots is adopted, while the number of modules constituting the machine is fixed to 10. Each module is an arc of 459 mm in length (1/10 of the stator circumference) and each pole will have a tangential length about 46 mm, which will be the base value for the PM arc hereinafter indicated in per unit values.

The electromagnetic design is executed through optimization runs performed considering a population size of 40 candidates iterated over 50 generations; the limits of the search space are reported in Table 1.

Table 1. Limits of the search space adopted for the optimization.

Parameter	Lower Bound	Upper Bound	Unit
Magnet arc	0.65	0.9	p.u.
Magnet thickness	10	20	mm
PCB thickness	1	3	mm

In order to evaluate the influence of the rotor and stator materials on the machine performance, four different combinations have been analyzed with the aid of the optimization tool.

The four combinations under investigation are reported in the following:

- Type A: machine with non-magnetic material for both stator and rotor yokes (ironless machine);
- Type B: machine with non-magnetic material for the stator yoke and ferromagnetic material (M-19 29 Ga) for the rotor yoke;
- Type C: machine with ferromagnetic material (M-19 29 Ga) for both stator and rotor yokes; and,
- Type D: machine with non-magnetic material for the rotor yoke and ferromagnetic material (M-19 29 Ga) for the stator yoke.

For each combination, an optimization run has been performed considering the same settings and the limits reported in Table 1.

The following Figures 12–15 report the main results of the four runs performed for the different machine configurations.

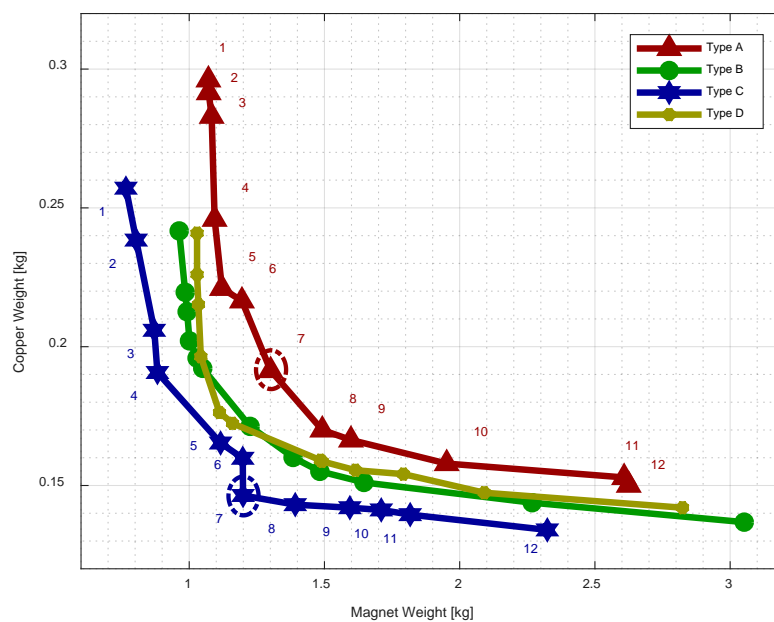


Figure 12. Pareto fronts obtained after the four optimization runs.

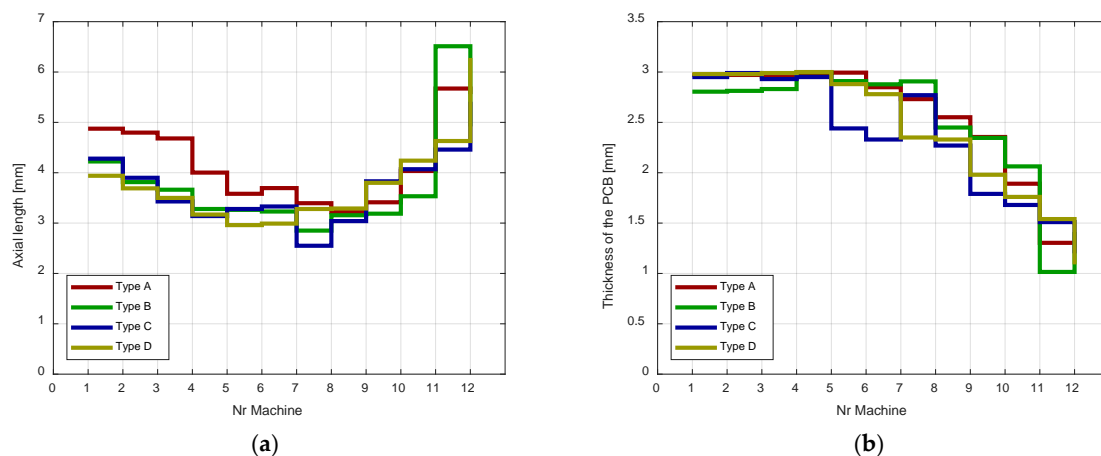
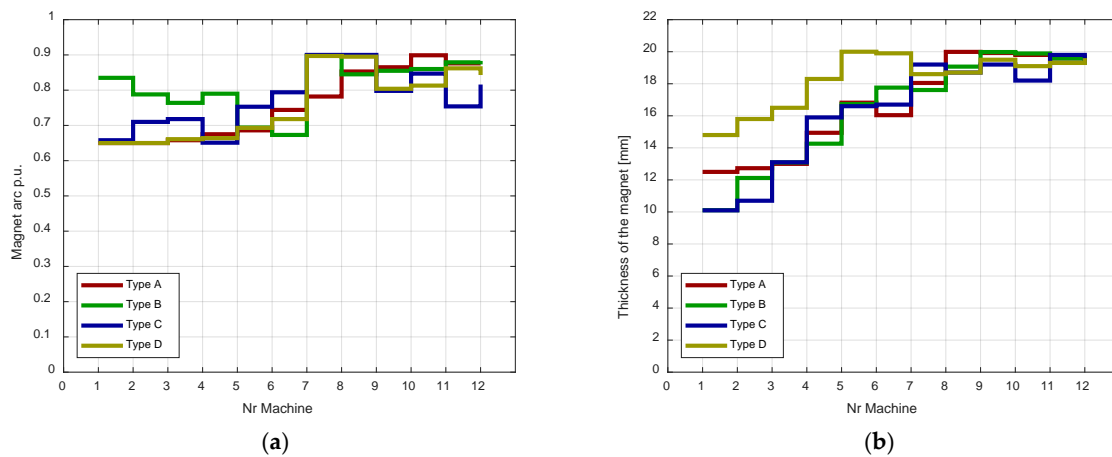
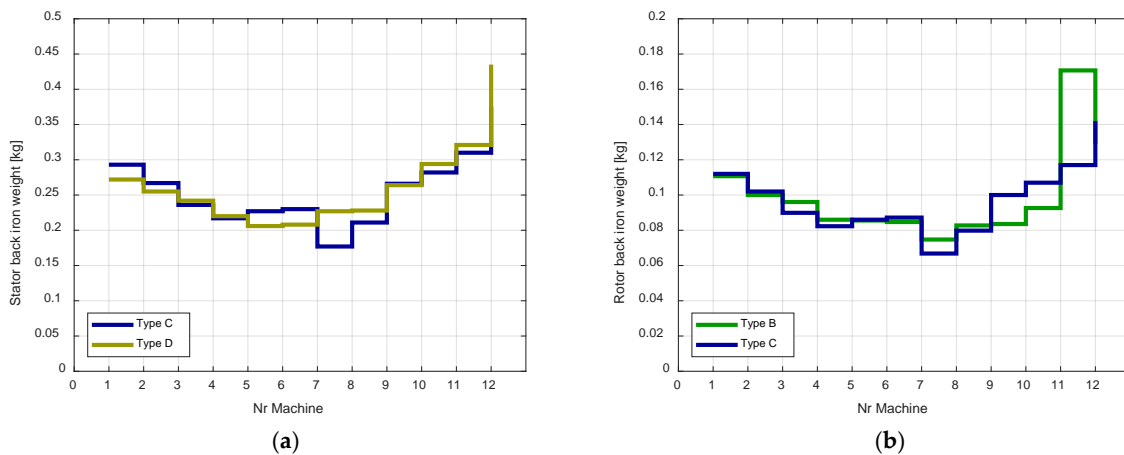


Figure 13. Axial length (a) and PCB thickness (b) of the machines belonging to the four Pareto fronts.

Figure 12 shows the Pareto fronts obtained after each run. For sake of easiness, the numbering of the machines is inserted for the outermost fronts; anyway, the other configurations follow the same logic (machine number 1 is the one with the greater copper weight and machine number 12 is the one with the lowest copper weight).



**Figure 14.** Permanent magnet arc (a) and thicknesses (b) of the machines belonging to the four Pareto fronts.



**Figure 15.** Stator (a) and rotor (b) magnetic yokes weights of the machines belonging to the Pareto fronts.

All of the candidate machines shown share the same electromagnetic torque (i.e., 14.4 Nm); as expected, machines with iron on both stator and rotor require less amount of permanent magnet and copper for the same output power with respect to completely ironless ones. In general, there is a minimum of the axial length of the machines in the middle of the Pareto fronts, between machines 7 and 9 (see Figure 13). Such machines present higher values of the PM arc and thickness (see Figure 14) but also minimize the iron quantity, as evidenced in Figure 15.

### 5.1. Comparison

Starting from the results shown in the previous paragraph, the two outermost Pareto fronts, corresponding to Type A (both stator and rotor ironless) and Type C (both stator and rotor with iron lamination) machines, are considered.

The machines n.7 of each front have been selected and accurately analyzed, at the rated conditions, through electromagnetic transient with motion FEA in order to compute the airgap field, the loss distribution, and the efficiency. The main results of this analysis are reported in Figure 16 and Table 2.

Both of the machines have low values of the inductances due to the large airgap; moreover, the power factor approaches one. The ironless machine (Type A) shows a slightly higher efficiency with respect to the Type C one. This is due to the larger amount of permanent magnet (+10%) and copper (+30%) of the first machine; moreover, the absence of ferromagnetic alloys for both the stator and rotor cores contributes to the reduction of the overall loss. Nevertheless, it is worth reminding that the final choice has to be a compromise between costs, performances, and simple manufacturability.

Considering large scale production, the reduced material cost and the lower mass of the rotating parts can be the main advantages of Type C machines.

**Table 2.** Characteristics of the two selected machines.

Parameter	N.7-Type A	N.7-Type C
Power [kW]	1	1
Electromagnetic torque [Nm]	14.4	14.4
Copper weight [kg]	0.19	0.15
Magnet weight [kg]	1.30	1.20
Thickness of the magnet [mm]	18.1	19.2
Thickness of the PCB [mm]	2.7	2.8
Axial length [mm]	3.4	2.6
Magnet arc [p.u.]	0.78	0.90
Copper loss [W]	15	11
Iron loss [W]	0	19
Efficiency [%]	98.5	97

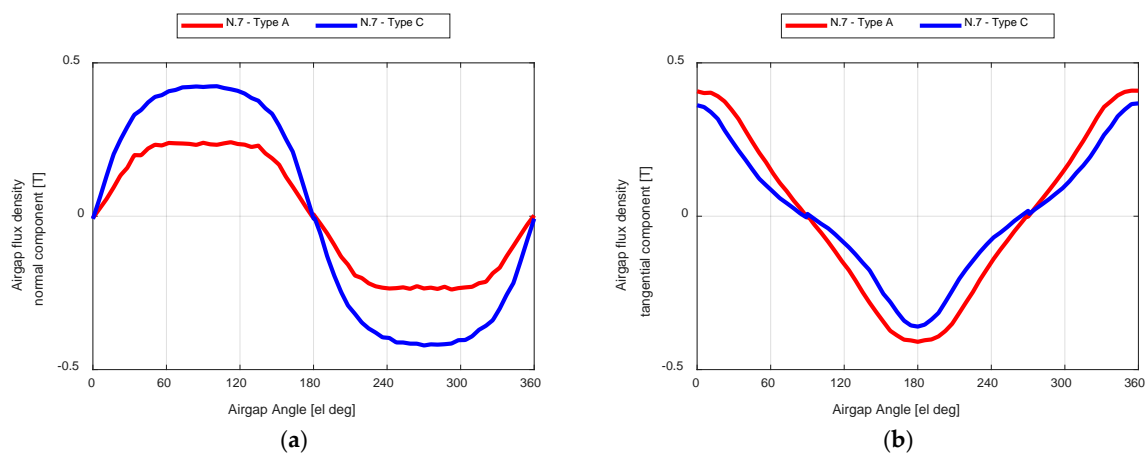


**Figure 16.** Airgap flux density of the two machines FE-analyzed. Normal (a) and tangential (b) components.

A further analysis on both the selected machines has been executed in order to point out their performance under different load conditions. Figures 17 and 18 report the main results obtained for the machine n.7-Type A and n.7-Type C, respectively: the losses distributions and the efficiency for different current values, expressed in per unit of the rated current, were FE-evaluated between no load condition and 100% overload condition.

Since the Type A machine is completely ironless and the rotational speed is quite low, almost all of the losses are in the stator windings and are proportional to the square of the current (Figure 17a). Moreover, due to the absence of iron parts, the torque is proportional to the phase current. This causes a decrease in the overall efficiency as the load increases, as highlighted in Figure 17b. As regards the machine n.7-Type C, almost the whole amount of iron losses is in the stator lamination; moreover, they are quite independent from the load current. The first bar in Figure 18a refers to a no-load FE simulation, highlighting that iron losses are mainly due to the PM flux for the considered current range. Due to the low amount of iron, the relation between output torque and phase current is almost linear in the considered range also in this case; therefore, efficiency presents a peak at rated conditions, but remains over 95% in the range  $0.5 I_n$  to  $2 I_n$ , as shown in Figure 18b.

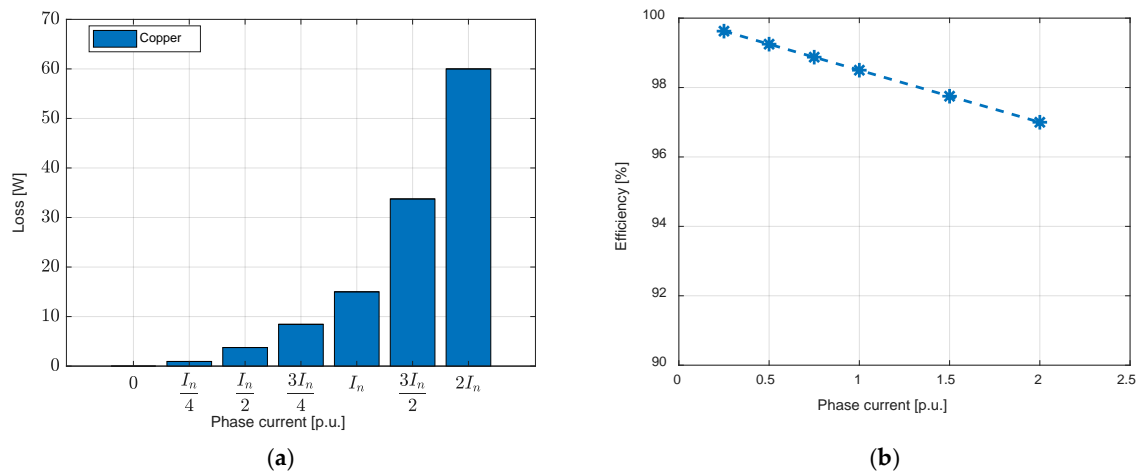


**Figure 17.** Losses distribution (a) and efficiency (b) for different load conditions for the machine n.7-Type A.

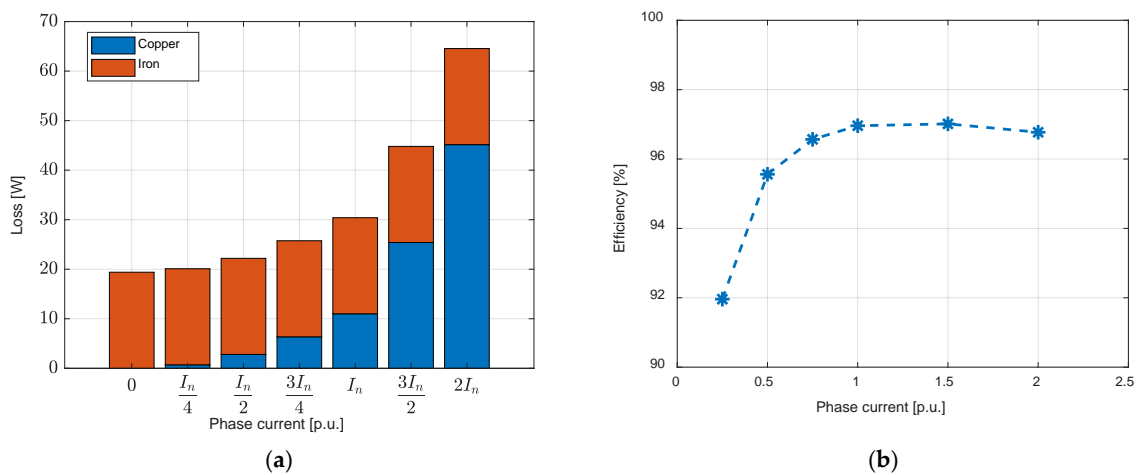


**Figure 18.** Losses distribution (a) and efficiency (b) for different load conditions for the machine n.7-Type C.

## 5.2. Scalability

Starting from the machine n.7-Type C (i.e., the one with both stator and rotor yokes made by ferromagnetic material), whose rated power is 1 kW, the scalability rules derived in Section 3 have been applied in order to quickly design machines with rated power halved and doubled. All the dimensions are obtained while considering a horizontal axis ducted turbine with a tip speed ratio equal to 5, which corresponds to  $C_p = 1$ , a wind speed equal to 10 m/s and a density of the air equal to  $1.22 \text{ kg/m}^3$ .

The two scaled machines are referred to as n.7-h (half-power machine) and n.7-d (double-power machine); both of them were obtained while considering the same values of magnet thickness, magnet arc and PCB thickness obtained, after the optimization, for the base machine n.7. The current density is the same for all the machines. The number of modules was adapted in order to find the best compromise between performance and manufacturing simplicity: finally, 8 and 12 modules were chosen for the half-power and the double-power machine, respectively. The main results are summarized in Table 3. As the target power of the turbine increases, the rotational speed reduces; nevertheless, the centrifugal force acting on the rotor rises due to the increased mass of the permanent magnet mounted on the rotor. Therefore, for higher values of the output power, the mechanical issues become more significant.

**Table 3.** Results of the scalability procedure.

Parameter	Starting Machine	Half-Power Machine	Double-Power Machine
Target Power [kW]	1	0.5	2
Turbine diameter [mm]	1440	1020	2040
Rotational speed [rpm]	663	937	468
Target torque [Nm]	14.4	5.1	40.8
Generator axial length [mm]	2.6	1.9	3.7
Copper weight [kg]	0.15	0.08	0.31
Magnet weight [kg]	1.20	0.64	2.55

Finally, in order to compare the machines obtained through the scaling procedure with optimally designed solutions, the automated design procedure was applied considering target values of the power equal to 0.5 kW and 2 kW, respectively. Figure 19 reports the two Pareto fronts found after the optimization plus the machines n.7-h and n.7-d, obtained from the machine n.7-Type C by applying the scalability rules. The machines represented in Figure 19a,b share the same torque, which is 5.1 Nm and 40.8 Nm, respectively. The machines that were obtained by applying the scalability rules are sub-optimal solutions, since they do not belong to the Pareto fronts; nevertheless, the values of their cost functions are not far from the optimal ones (the difference is less than 10%). Since this result was obtained without performing a dedicated optimization, it can be considered a good compromise between performance and computational burden.

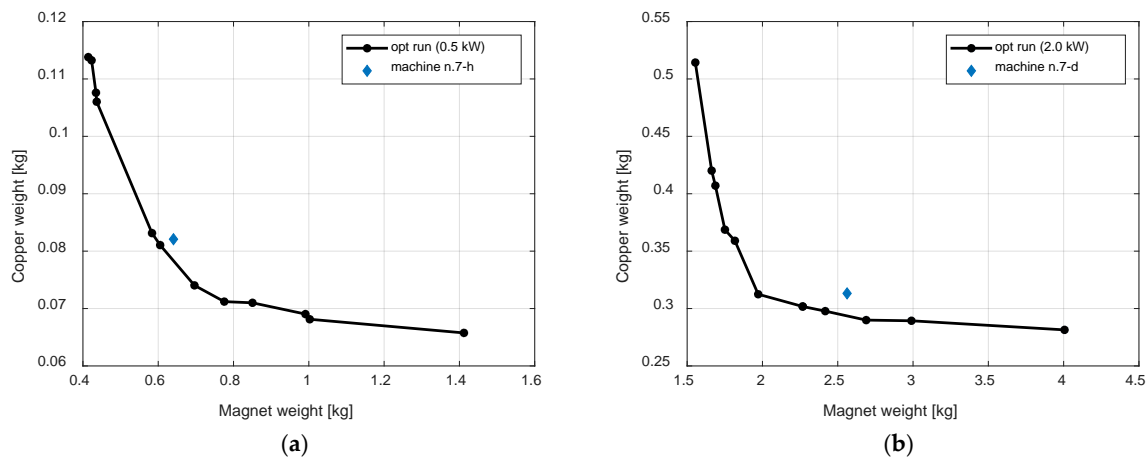


**Figure 19.** Comparison between optimally designed machines and scaled machines with half-power (a) and double-power (b) with respect to the base machine.

## 6. Conclusions

This work was focused on the optimal design of annular PM machines for small-scale direct-drive ducted wind turbines. An automated tool that is based on genetic algorithms and fast finite element analysis has been developed in order to quickly design the electrical machine, starting from the torque requirements. Moreover, simple scalability rules have been provided in order to adapt the geometric dimensions of the machine to the required output power. The adoption of PCB concentrated windings in order to increase the current capacity and reduce the copper weight has been investigated together with the influence of the rotor\stator materials on the torque capability and on the cost of the active parts (i.e., copper and PMs).

The proposed tool, even though quite accurate, is very quick with a reduced computational burden; moreover, it is based on open-source software for the finite element analysis. Therefore, it can constitute a valid support for the electrical machine designer.

The main contribution of this work, with respect to the existing literature, is twofold: firstly, the adoption of annular PM machines that are applied to aerogenerators is investigated; secondly,

an original automated design procedure aimed at minimizing the weight and the cost of the electrical generator is presented. Finally, the use of computationally expensive design techniques, based on FEA and optimization algorithms, is limited thanks to the proposed scalability rules.

**Author Contributions:** The authors equally contributed to this article in terms of conceiving, theoretical analysis, numerical simulations, paper writing.

**Funding:** This work was supported by the project “Wind Micro-Turbine Networks for Urban Areas” (in Italian “Reti di microturbine eoliche per la produzione diffusa di energia in ambito urbano”)—Fondazione Puglia, Italy.

**Acknowledgments:** The authors would like to thank P. Caldori for his help in the realization of the Matlab code for the optimization of the electrical machine design.

**Conflicts of Interest:** The authors declare no conflict of interest.

## Nomenclature

### Symbols

$A$	Wind turbine rotor swept area
$C$	Rotor circumference
$C_p$	Power coefficient
$D$	Rotor diameter
$F$	Force at airgap
$i_{sdq}$	Stator current in the dq-reference frame
$L$	Axial length
$P$	Output power
$R$	Rotor radius
$T$	Output torque
$\lambda$	Tip Speed Ratio
$\lambda_{dq}$	Flux linkage in the dq-reference frame
$\rho$	Air density
$R_S$	Stator resistance
$T_{target}$	Target torque
$v_a$	Wind speed upstream the streamtube
$v_p$	Wind speed at the rotor
$v_O$	Wind speed downstream the streamtube
$v_{sdq}$	Stator voltage in the dq-reference frame
$\omega$	Rotational speed

### Acronyms

CP	Combined Population
CFD	Computational Fluid Dynamic
DAWT	Diffuser-Augmented Wind Turbines
DC	Direct Current
DL	Double Layer
FE	Finite Element
FEA	Finite Element Analysis
FEMM	Finite Element Method Magnetics
NSGA	Nondominated Sorting Genetic Algorithm
PCB	Printed Circuit Board
PM	Permanent Magnet
p.u.	Per Unit
S-HAWT	Shrouded Horizontal Axis Wind Turbines
SL	Single Layer

## References

1. Wu, Y.K.; Tsai, C.Z.; Li, Y.H. Design of wind power generators: Summary and comparison. In Proceedings of the 2018 IEEE International Conference on Applied System Invention (ICASI), Chiba, Japan, 13–17 April 2018; pp. 1314–1317.
2. Cuesta, A.B.; Gomez-Gil, F.J.; Fraile, J.V.M.; Rodríguez, J.A.; Calvo, J.R.; Vara, J.P. Feasibility of a Simple Small Wind Turbine with Variable-Speed Regulation Made of Commercial Components. *Energies* **2013**, *6*, 3373–3391. [[CrossRef](#)]
3. Blaabjerg, F.; Liserre, M.; Ma, K. Power Electronics Converters for Wind Turbine Systems. *IEEE Trans. Ind. Appl.* **2012**, *48*, 708–719. [[CrossRef](#)]
4. Stiebler, M. *Wind Energy Systems for Electric Power Generation*; Springer: Berlin/Heidelberg, Germany, 2008.
5. Blaabjerg, F.; Ma, K. Wind Energy Systems. *Proc. IEEE* **2017**, *105*, 2116–2131. [[CrossRef](#)]
6. Potgieter, J.H.J.; Kamper, M.J. Double PM-Rotor, Toothed, Toroidal-Winding Wind Generator: A Comparison with Conventional Winding Direct-Drive PM Wind Generators over a Wide Power Range. *IEEE Trans. Ind. Appl.* **2016**, *52*, 2881–2891. [[CrossRef](#)]
7. Artal-Sevil, J.S.; Dufo, R.; Domínguez, J.A.; Bernal-Agustín, J.L. Small wind turbines in smart grids. Transformation of electrical machines in permanent magnet synchronous generators. In Proceedings of the 2018 Thirteenth International Conference on Ecological Vehicles and Renewable Energies (EVER), Monte-Carlo, Monaco, 10–12 April 2018; pp. 1–8.
8. Zeinali, R.; Ertan, H.B.; Yamali, C.; Tarvirdilu-Asl, R. Magnetically geared direct drive wind generator thermal analysis. In Proceedings of the 2017 International Conference on Optimization of Electrical and Electronic Equipment (OPTIM) & 2017 International Aegean Conference on Electrical Machines and Power Electronics (ACEMP), Brasov, Romania, 25–27 May 2017; pp. 462–469.
9. Polinder, H.; van der Pijl, F.F.A.; de Vilder, G.J.; Tavner, P.J. Comparison of direct-drive and geared generator concepts for wind turbines. *IEEE Trans. Energy Convers.* **2006**, *21*, 725–733. [[CrossRef](#)]
10. Li, H.; Chen, Z. Overview of different wind generator systems and their comparisons. *IET Renew. Power Gener.* **2008**, *2*, 123–138. [[CrossRef](#)]
11. Baroudi, J.A.; Dinavahi, V.; Knight, A.M. A review of power converter topologies for wind generators. *Renew. Energy* **2007**, *32*, 2369–2385. [[CrossRef](#)]
12. Yuan, T.; Yang, N.; Zhang, W.; Cao, W.; Xing, N.; Tan, Z.; Li, G. Improved Synchronous Machine Rotor Design for the Easy Assembly of Excitation Coils Based on Surrogate Optimization. *Energies* **2018**, *11*, 1311. [[CrossRef](#)]
13. Higuchi, T.; Yokoi, Y.; Abe, T.; Sakimura, K. Design Analysis of a Novel Synchronous Generator for Wind Power Generation. *Machines* **2014**, *2*, 202–218. [[CrossRef](#)]
14. Stamenkovic, I.; Milivojevic, N.; Schofield, N.; Krishnamurthy, M.; Emadi, A. Design, Analysis, and Optimization of Ironless Stator Permanent Magnet Machines. *IEEE Trans. Power Electron.* **2013**, *28*, 2527–2538. [[CrossRef](#)]
15. Stegmann, J.A.; Kamper, M.J. Design Aspects of Double-Sided Rotor Radial Flux Air-Cored Permanent-Magnet Wind Generator. *IEEE Trans. Ind. Appl.* **2011**, *47*, 767–778. [[CrossRef](#)]
16. Peng, G.; Wei, J.; Shi, Y.; Shao, Z.; Jian, L. A Novel Transverse Flux Permanent Magnet Disk Wind Power Generator with H-Shaped Stator Cores. *Energies* **2018**, *11*, 810. [[CrossRef](#)]
17. Jamali Arand, S.; Ardebili, M. Multi-objective design and prototyping of a low cogging torque axial-flux PM generator with segmented stator for small-scale direct-drive wind turbines. *IET Electr. Power Appl.* **2016**, *10*, 889–899. [[CrossRef](#)]
18. IPC-2221. *Generic Standard for Printed Wiring Boards*. Available online: <http://shop.ipc.org/IPC-2221B-English-P> (accessed on 21 September 2018).
19. Cupertino, F.; Ettore, S. Torque production capabilities of electrical machines with planar windings. In Proceedings of the 38th Annual Conference on IEEE Industrial Electronics Society (IECON 2012), Montreal, QC, Canada, 25–28 October 2012; pp. 2080–2085.
20. Yan, G.J.; Hsu, L.Y.; Wang, J.H.; Tsai, M.C.; Wu, X.Y. Axial-Flux Permanent Magnet Brushless Motor for Slim Vortex Pumps. *IEEE Trans. Magn.* **2009**, *45*, 4732–4735. [[CrossRef](#)]
21. Moury, S.; Iqbal, M.T. A permanent magnet generator with PCB stator for low speed marine current applications. In Proceedings of the 2009 1st International Conference on the Developments in Renewable Energy Technology (ICDRET), Dhaka, Bangladesh, 17–19 December 2009; pp. 1–4.

22. Hsu, L.Y.; Yan, G.J.; Tsai, M.C. Novel flexible printed circuit windings for slotless linear motor design. In Proceedings of the 2010 International Conference on Electrical Machines and Systems, Incheon, Korea, 10–13 October 2010; pp. 1578–1582.
23. Ustun, O.; Tuncay, R.N. Design, analysis, and control of a novel linear actuator. *IEEE Trans. Ind. Appl.* **2006**, *42*, 1007–1013. [[CrossRef](#)]
24. Hu, J.-F.; Wang, W.-X. Upgrading a Shrouded Wind Turbine with a Self-Adaptive Flanged Diffuser. *Energies* **2015**, *8*, 5319–5337. [[CrossRef](#)]
25. Ohya, Y.; Karasudani, T. A shrouded wind turbine generating high output power with wind-lens technology. *Energies* **2010**, *3*, 634–649. [[CrossRef](#)]
26. Khamlaj, T.A.; Rumpfkeil, M.P. Theoretical analysis of shrouded horizontal axis wind turbines. *Energies* **2017**, *10*, 38. [[CrossRef](#)]
27. Werkle, M.J.; Presz, W.M., Jr. Ducted wind/water turbines and propellers revisited. *J. Propuls. Power* **2008**, *24*, 1146–1150. [[CrossRef](#)]
28. Torresi, M.; Postiglione, N.; Filianoti, P.F.; Fortunato, B.; Camporeale, S.M. Design of a ducted wind turbine for offshore floating platforms. *Wind Eng.* **2016**, *40*, 468–474. [[CrossRef](#)]
29. Deb, K.; Pratap, A.; Agarwal, S.; Meyarivan, T. A fast and elitist multiobjective genetic algorithm: NSGA-II. *IEEE Trans. Evol. Comput.* **2002**, *6*, 182–197. [[CrossRef](#)]
30. Meeker, D.C. Finite Element Method Magnetics, Version 4.2. Available online: <http://www.femm.info> (accessed on 3 May 2017).
31. Meeker, D.; Bianchi, N.; Gyselinck, J.; Sabariego, R.V.; Alberti, L.; Pellegrino, G.; Cupertino, F. Electrical machine analysis using free software. In Proceedings of the 2017 IEEE Energy Conversion Congress and Exposition (ECCE), Cincinnati, OH, USA, 1–5 October 2017; pp. 1–289.
32. Fatemi, A.; Ionel, D.M.; Demerdash, N.A.O.; Nehl, T.W. Fast Multi-Objective CMODE-Type Optimization of PM Machines Using Multicore Desktop Computers. *IEEE Trans. Ind. Appl.* **2016**, *52*, 2941–2950. [[CrossRef](#)]
33. Cupertino, F.; Pellegrino, G.; Gerada, C. Design of Synchronous Reluctance Motors with Multiobjective Optimization Algorithms. *IEEE Trans. Ind. Appl.* **2014**, *50*, 3617–3627. [[CrossRef](#)]
34. Di Nardo, M.; Galea, M.; Gerada, C.; Palmieri, M.; Cupertino, F. Multi-physics optimization strategies for high speed synchronous reluctance machines. In Proceedings of the 2015 IEEE Energy Conversion Congress and Exposition (ECCE), Montreal, QC, Canada, 20–24 September 2015; pp. 2813–2820.
35. Rosu, M.; Zhou, P.; Lin, D.; Ionel, D.M.; Popescu, M.; Blaabjerg, F.; Rallabandi, V.; Staton, D. Automated Optimization for Electric Machines. In *Multiphysics Simulation by Design for Electrical Machines, Power Electronics and Drives*; Wiley-IEEE Press: Hoboken, NJ, USA, 2018; Volume 1, p. 312.
36. Cupertino, F.; Palmieri, M.; Pellegrino, G. Design of high-speed synchronous reluctance machines. In Proceedings of the 2015 IEEE Energy Conversion Congress and Exposition (ECCE), Montreal, QC, Canada, 20–24 September 2015; pp. 4828–4834.
37. Cupertino, F.; Leuzzi, R.; Monopoli, V.G.; Cascella, G.L. Maximisation of power density in permanent magnet machines with the aid of optimisation algorithms. *IET Electr. Power Appl.* **2018**, *12*, 1067–1074. [[CrossRef](#)]
38. Duan, Y.; Ionel, D.M. A Review of Recent Developments in Electrical Machine Design Optimization Methods with a Permanent-Magnet Synchronous Motor Benchmark Study. *IEEE Trans. Ind. Appl.* **2013**, *49*, 1268–1275. [[CrossRef](#)]
39. Goldberg, D.E. *Genetic Algorithms in Search, Optimization, and Machine Learning*, 1st ed.; Addison-Wesley: Boston, MA, USA, 1989; ISBN 0201157675.

